

Measurement of B^+ and B_s^0 meson cross sections in pp collisions at the LHC

Simão Costa^{1,a} and Jean Luo^{2,b}

¹Instituto Superior Técnico, Lisboa, Portugal

²Imperial College London, London, United Kingdom

Project supervisor: N. Leonardo, H. Legoinha

October 19, 2022

Abstract. The differential production cross sections of both B^+ and B_s^0 mesons in pp collisions have been measured as part of the study of the quark gluon plasma. The measurements are performed as function of the meson's rapidity and event multiplicity. The analysis is based on $\sqrt{s} = 5$ TeV pp data collected by CMS, with an integrated luminosity of 302.3 pb^{-1} . The raw signal yields are extracted by fitting the invariant mass spectra of the particles produced at the end of the selected decay chain for each meson. The quality of the fits has been verified by χ^2 and pull tests as well as stability across bins. The results here presented are preliminary.

KEYWORDS: LHC, CMS, quark gluon plasma, differential cross section, B mesons

1 Introduction

1.1 The Quark Gluon Plasma

Quark gluon plasma (QGP) is a very exotic state of matter, in which quark and gluons become 'free' instead of being bound within hadrons. This state of matter only exists under extreme conditions: for normal baryon density, the phase transition temperature from normal hadronic matter to QGP is around $T = 150$ MeV (equivalent to $T = 1.7 \times 10^{12}$ K) [1]. The study of such matter not only completes the big picture of quantum chromodynamics (QCD), but also links directly to the understanding of the very early universe, since it is believed that the universe was entirely filled by QGP within a few μs after the Big Bang [1]. At the LHC, droplets of QGP can be produced by ultrarelativistic heavy ion collisions (URHICs) and detected by the Compact Muon Solenoid (CMS) detector at the LHC.

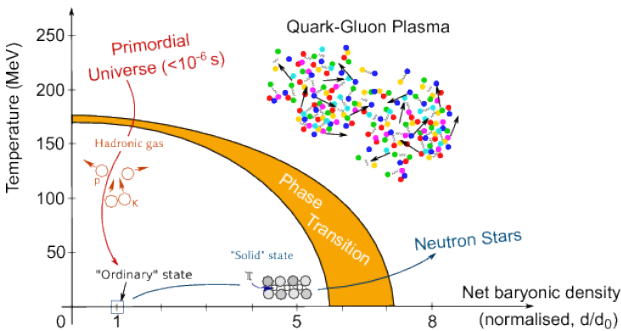


Figure 1. The QCD phase diagram.

This work aims to study how the presence of QGP affects the b-quark hadronisation process. This is done by measuring the production cross section, σ_{pp} , of both B^+ and B_s^0 mesons in pp collisions, which serve as a reference for lead-lead (PbPb) collisions [2, 3], thus allowing

to identify the QGP effects. The differential cross section is given by

$$\frac{d\sigma}{d\phi} = \frac{1}{\epsilon LB} \frac{dN_S}{d\phi}, \quad (1)$$

where ϕ is the differential variable used for the analysis (rapidity, multiplicity), ϵ is the efficiency times acceptance of the detector, L is the integrated luminosity of the data set, B is the branching fraction of the decay chain and N_S is the number of signal events. The values of ϵ are determined from Monte Carlo simulations of the decay process and detector, whereas N_S is extracted by fitting the data. These cross sections from pp collisions (which do not produce QGP) are then compared to the ones obtained from the PbPb collisions (which produce QGP), by computing the nuclear modification factor, R_{AA} , from which the properties of QGP can be learnt [3]:

$$R_{AA} = \frac{1}{\langle N_{col} \rangle} \frac{(\frac{d\sigma}{d\phi})_{PbPb}}{(\frac{d\sigma}{d\phi})_{pp}} \quad (2)$$

where $\frac{1}{\langle N_{col} \rangle}$ accounts for the higher number of colliding nuclei in PbPb, $(\frac{d\sigma}{d\phi})_{PbPb}$ and $(\frac{d\sigma}{d\phi})_{pp}$ are the differential production cross section in PbPb and pp collisions, respectively.

The analysis is based on the $\sqrt{s} = 5$ TeV pp dataset collected by CMS in 2017 and performed as function of two variables: rapidity of the B mesons, y , and the event multiplicity, N_{ch} (see Fig. 2): y is related to the angular position at which the meson is reconstructed, whereas N_{ch} is the number of charged particles detected in the collision, which hence gives information about the environment in which the b quark hadronizes.

1.2 B mesons as probes of the QGP

B mesons are formed by a anti-bottom quark and another flavour of quark (apart from top quark). They can be used as probes of the QGP for two main reasons: B mesons have a relatively larger lifetime so that they can displace further from the point of collisions, and hence the B mesons can be easily distinguished from the other particles; they are

^ae-mail: simao.costa@tecnico.ulisboa.pt

^be-mail: jean.luo@laposte.net

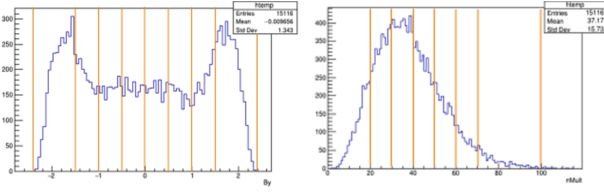


Figure 2. (left) The data of rapidity, the binning is (-2.4, -1.5, -1.0, -0.5, 0.0, 0.5, 1.0, 1.5, 2.0, 2.4). (right) The data of multiplicity, the binning is (0, 20, 30, 40, 50, 60, 70, 100).

very massive mesons hence the thermal production can be ignored [4].

For each of the B mesons used for analysis, B^+ and B_s^0 , a specific decay channel is selected, as depicted on Fig. (3) and Fig. (4) respectively. The J/ψ and ϕ candidates are reconstructed as $J/\psi \rightarrow \mu^+\mu^-$ and $\phi \rightarrow K^+K^-$. The complete decays of the B mesons are thus given by $B^+ \rightarrow J/\psi K^+ \rightarrow \mu^+\mu^-K^+$ and $B_s^0 \rightarrow J/\psi \phi \rightarrow \mu^+\mu^-K^+K^-$.

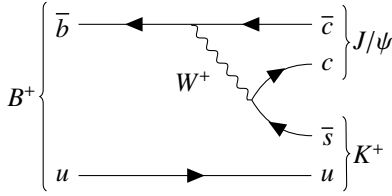


Figure 3. The leading-order Feynman diagram of the studied B^+ meson decay, $B^+ \rightarrow J/\psi K^+$.

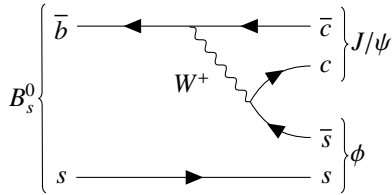


Figure 4. The leading-order Feynman diagram of the studied B_s^0 meson decay, $B_s^0 \rightarrow J/\psi \phi$.

2 Mass Fit

2.1 The Extended Unbinned Maximum Likelihood method and the nominal model

The Extended Unbinned Maximum Likelihood method [5] is used to fit the invariant mass spectra of the reconstructed final states. The parameters that best describe the data, $\vec{\lambda}$, can be obtained by maximizing the likelihood, $\mathcal{L}(\vec{\lambda})$:

$$\mathcal{L}(\vec{\lambda}) = \frac{N^{N_{obs}} e^{-N}}{N_{obs}!} \prod_{i=1}^{N_{obs}} l(m_i, \vec{\lambda}) \quad (3)$$

where N is the actual total number of events, N_{obs} is the estimated total number, m_i is the invariant mass of the i -th event and l is the model i.e. a probability distribution function (PDF) describing the shape of the data.

The nominal model used for fitting the data is given by the sum of a double-Gaussian (signal) and an exponential function (combinatorial background):

$$l(m_i, \vec{\lambda}) = N_s \left(\frac{\alpha}{\sqrt{2\pi}\sigma_1} e^{-\frac{(m_i-\mu_1)^2}{2\sigma_1^2}} + \frac{(1-\alpha)}{\sqrt{2\pi}\sigma_2} e^{-\frac{(m_i-\mu_2)^2}{2\sigma_2^2}} \right) + N_{cb}\lambda_{cb}e^{-\lambda_{cb}m_i} + N_{peak}\Phi_{peak} + N_{part}\Phi_{part} \quad (4)$$

where α is the weight of each Gaussian function, σ_i and μ_i are respectively the width and the mean of the i -th Gaussian, λ_{cb} is the decay factor of the exponential background, N_s is the number of signal events which are the parameter of interest that will be used for the further analysis, N_{cb} is the number of combinatorial background candidates.

For the B^+ case, additional background components arise. Sometimes, a K^+ from the B_s^0 decay may be missed, and the event may be thus misreconstructed as a B^+ meson. This results in a partially reconstructed background in the B^+ candidate mass spectrum (which because a particle is missed lies to the left of the signal peak). Additionally, the decay $B^+ \rightarrow J/\psi\pi^+$ may mimic the signal [4], when a π meson is misidentified as a K meson.¹ This decay is similar to the decay in Fig.(3), but instead of the W^+ boson decaying into a charm and anti-strange quark it decays into a charm and anti-down quark. This decay is suppressed because the CKM matrix (which governs the relative strength of these interactions), being very close to the identity, suppresses transitions between different generations of quarks, such as the one occurring in the latter process. The last two terms in Eq.(4) model these additional background components (which only appear for the B^+ case), being N_{peak} the number of peaking background events, N_{part} the number of partially reconstructed background events and Φ_{peak} and Φ_{part} the corresponding normalized models. For the peaking background we have chosen a Gaussian function to model the data and an error function to model the partially reconstructed background.

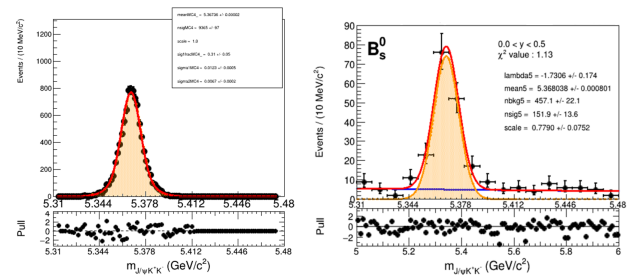


Figure 5. (left) The B_s^0 nominal fit to the MC simulation, shown for the bin $0.0 < y < 0.5$. The model used for the signal is a double Gaussian, with the fitted function being displayed by the red curve. (right) The nominal fit to the actual data, where the background model is now added, and the signal model obtained from the MC fit (left) is fixed. The box underneath shows the results of the pull test; the value of the χ^2 test is also shown.

¹We refer to this decay as the peaking background.

2.2 The fitting procedure

For each variable, the data is split into bins (see Fig. 2 for the binning adopted), and the data inside each bin is then fitted. Before fitting the actual invariant mass spectra of data, the fit is first performed to a signal-only spectra generated by Monte Carlo (MC) simulations (see Figure 5, left), from which we can obtain the parameters describing the shape of the function. These parameters are then kept fixed in the fit to the data, where the background model is included. The raw signal yield, N_S , is extracted from the fit to data.

The results obtained from the fits are validated using two statistical methods: χ^2 test and pull test. From the normalised χ^2 value, the information about the overall quality of the fits can be readily obtained. The pull test gives information about whether each data point in the fit is statistically well described by the curve across the fitting range (see bottom of Fig. 5, right).

2.3 Systematic uncertainties

Apart from the chosen nominal model, there are other possible models that can be used to describe the signal and the background; these alternative models are referred to as systematic variations. The raw signal yields obtained from these variations are potentially different to those from the nominal model, and these differences (in % relative to the nominal model) correspond to systematic uncertainties for the raw signal yield.

In this analysis, four signal variations (triple Gaussian, Gaussian + crystal ball, double crystal ball and fixed mean²) and three background variations (1st- order polynomial, 2nd-order polynomial and mass range) are used. The procedure is done for each meson and for each analysis bin.

2.4 Mass resolution

The mass resolution given by the width of the peak is computed as the weighted average of σ^2 's for the nominal model. The detector resolution is optimal in the central region (small $|y|$) and degrades towards the forward region (large $|y|$) in a symmetric way, as shown in Fig. 6. This happens due to the fact that the higher the rapidity $|y|$ is the more matter the particles will have to traverse, undergoing more multiple scattering and thus losing precision in the process.

3 Differential Signal Yield

To calculate the differential signal yields, the yields of each bin were obtained and then normalized by the width of the respective bin. This scaling is applied to both the central value and uncertainties. The systematic uncertainty is computed as the maximum of the signal and background

²When doing the fitting to the data we use the results of the fitting to the MC data as initial values for the parameters of our model, fixing some of these parameters depending on the model used. The fixed mean model is therefore a normal two-Gaussian model but where the mean parameter is fixed from the MC fit.

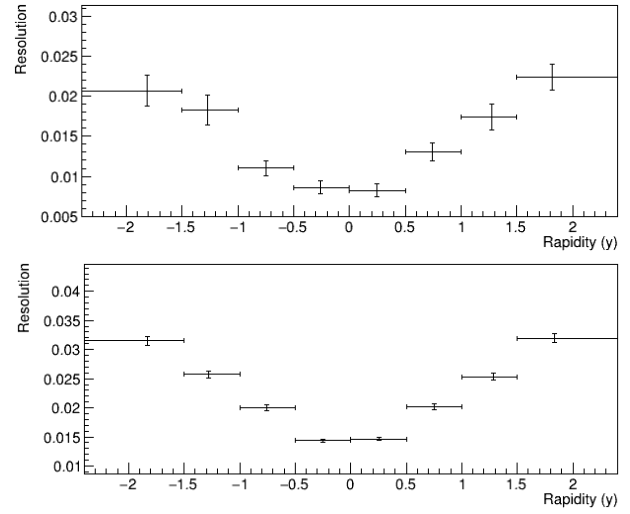


Figure 6. Mass resolution as function of rapidity for B_S^0 (top) and B^+ (bottom).

variations relative to the nominal yields. The results can be seen in Figs. 8 and 9.

It is worth noticing that, as the other plots also suggest, the error bars for B^+ are smaller than those of B_S^0 , i.e. B^+ measurements have a higher precision.

4 Detector efficiency

The total efficiency, ϵ , accounts for signal candidates that were not reconstructed or were rejected by the selection cuts used in the analysis. We can obtain this value from MC simulations by dividing the total number of events where selection cuts were performed [4], N^{cuts} , by that without any cuts, N^{total} ,

$$\epsilon = \frac{N^{cuts}}{N^{total}}. \quad (5)$$

The inverse of the total efficiency can be seen for the B_S^0 meson on Fig. 7, as function of rapidity and multiplicity.

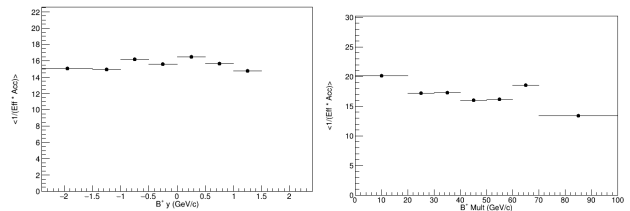


Figure 7. The inverse of the total efficiency, $\frac{1}{\epsilon}$, for the B_S^0 meson as function of rapidity (left) and multiplicity (right).

5 Cross Section

Based on the previous results of raw signal yields and efficiencies, the production cross sections can be calculated, following Eq. 1. The results are shown in Fig. 10.

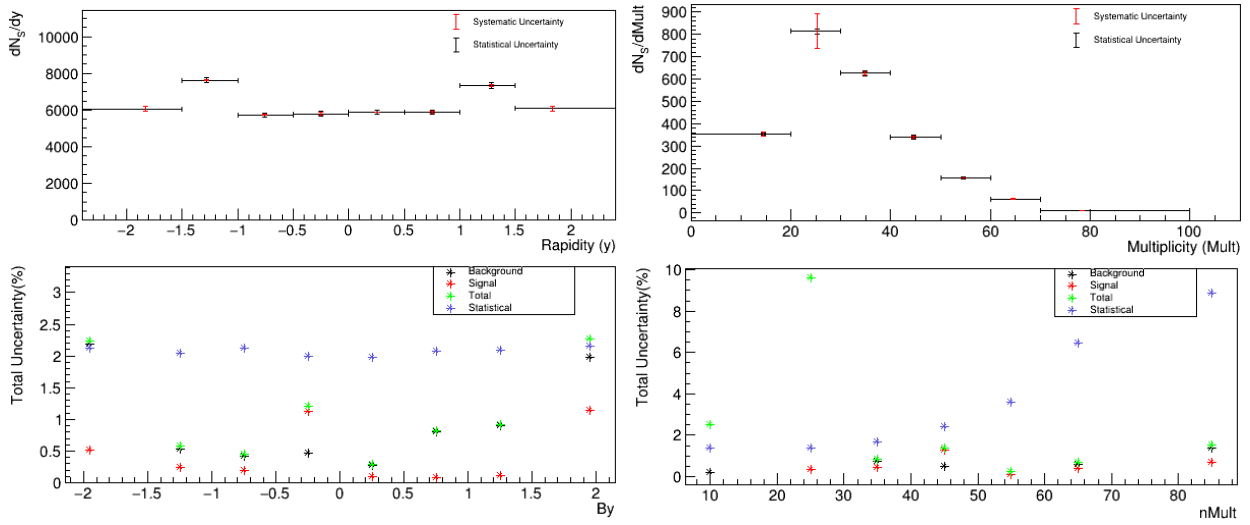


Figure 8. Fit results for the B^+ meson. Differential signal yields versus meson rapidity (top left) and event multiplicity (top right). Systematic error plots for rapidity (bottom left) and multiplicity (right). The signal and background systematic errors are each taken as the highest value of all of the respective variations, and the total error is the square root of the square sum of both of these errors.

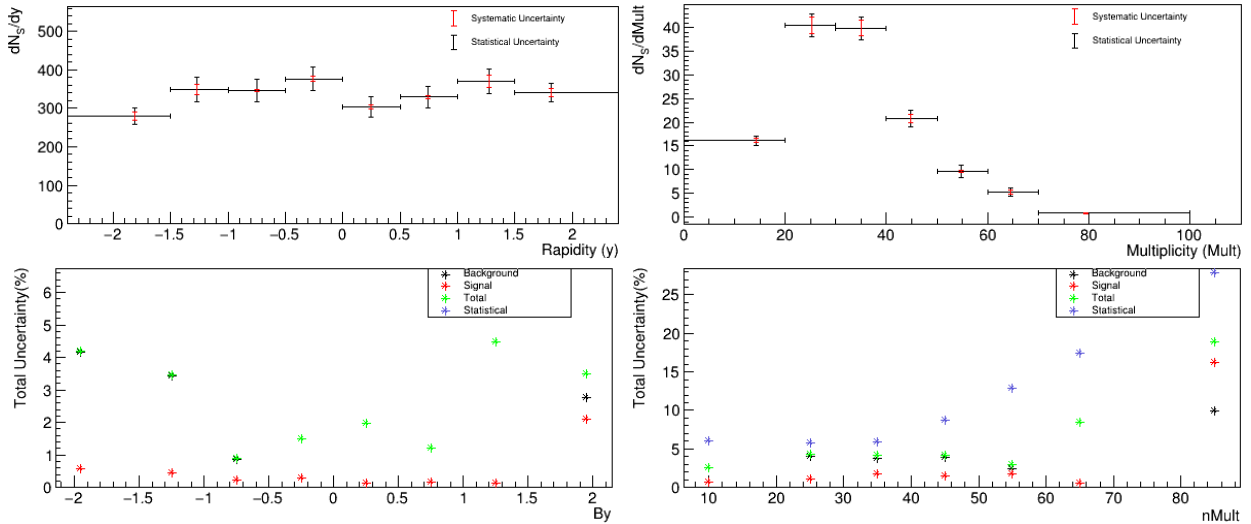


Figure 9. Fit results for the B_S^0 meson. Differential signal yields versus meson rapidity (top left) and event multiplicity (top right). Systematic error plots for rapidity (bottom left) and multiplicity (right). The signal and background systematic errors are each taken as the highest value of all of the respective variations, and the total error is the square root of the square sum of both of these errors.

6 Conclusions

Preliminary results are presented for the B_S^0 and B^+ meson production cross sections as function of meson rapidity and event multiplicity in pp collisions at $\sqrt{s} = 5$ TeV. The more detailed documentation of the work is provided as an internal CMS Analysis Note [6].

The results here attained may be used to test theory predictions. The cross section ratios for the two mesons provide insights into the fragmentation mechanisms of b quarks in vacuum. Together with corresponding results obtained for PbPb collisions, these results allow to determine the nuclear modification factors, R_{AA} . The analysis may be further extended to include additional differential variables, additional mesons, or to probe the lower p_T re-

gion giving us even more insight into the hadronization processes of quarks and the properties of the QGP.

7 Acknowledgements

We would like to express our gratitude towards Prof. Nuno Leonardo for his tremendous effort made on teaching and guiding us throughout the internship, and giving us opportunities to get involved in this very interesting and frontier research project.

Our thanks and appreciations also go to Mr. Henrique Legoinha who patiently helped us getting familiar with the tools we needed, he also answered our questions and provided us with useful suggestions about solving the problems encountered whilst completing the project.

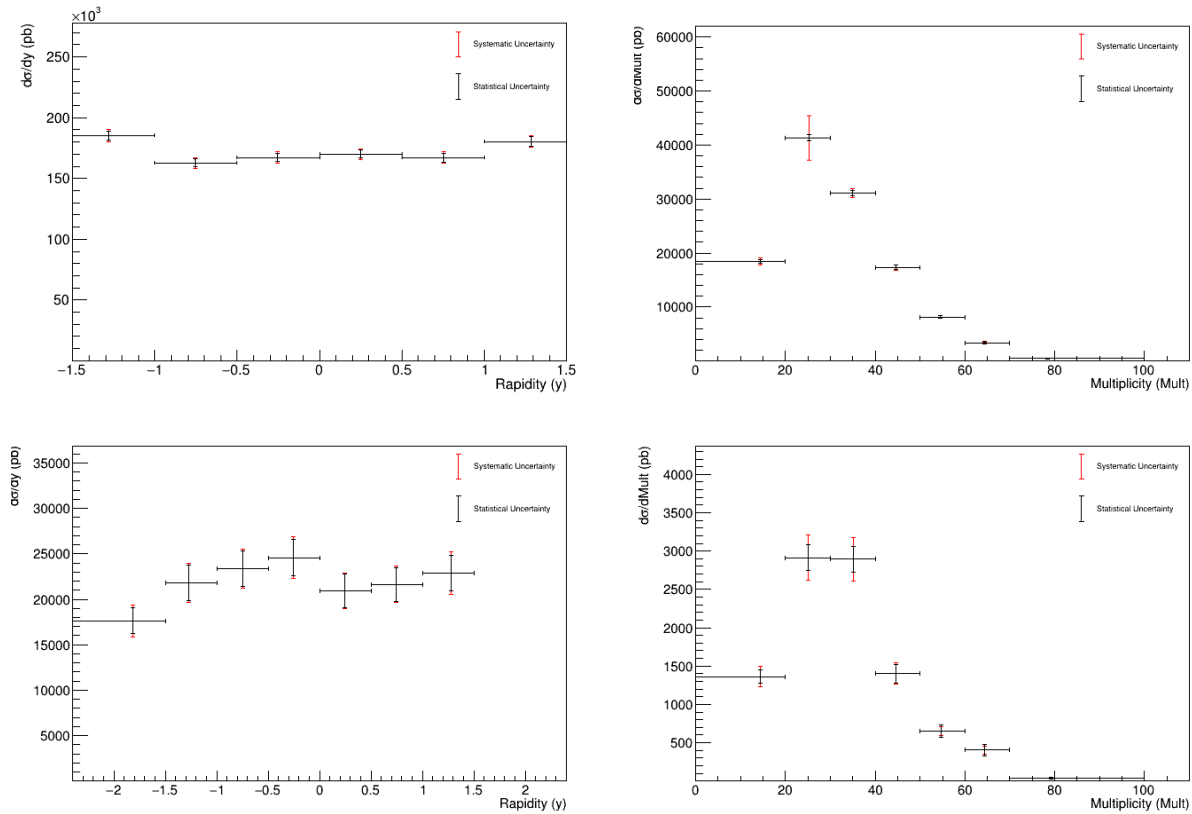


Figure 10. Differential cross section calculated based on the previous results for both B^+ meson (top row) and B_s^0 (bottom row), versus rapidity (left column) and multiplicity (right column).

References

- [1] Wit Busza, Krishna Rajagopal, and Wilke van der Schee. “Heavy Ion Collisions: The Big Picture and the Big Questions”. In: *Annual Review of Nuclear and Particle Science* 68.1 (Oct. 2018), pp. 339–376. doi: 10.1146/annurev-nucl-101917-020852. URL: <https://doi.org/10.1146/annurev-nucl-101917-020852>.
- [2] CMS Collaboration. “Observation of B_s^0 mesons and measurement of the B_s^0/B^+ yield ratio in PbPb collisions at $\sqrt{s_{NN}} = 5.02$ TeV”. In: *Phys. Lett. B* 829 (2022), p. 137062. doi: 10.1016/j.physletb.2022.137062. arXiv: 2109.01908 [hep-ex].
- [3] CMS Collaboration. “Measurement of the B^\pm meson nuclear modification factor in Pb-Pb collisions at $\sqrt{s_{NN}} = 5.02$ TeV”. In: *Phys. Rev. Lett.* 119 (15 Oct. 2017), p. 152301. doi: 10.1103/PhysRevLett.119.152301. URL: <https://link.aps.org/doi/10.1103/PhysRevLett.119.152301>.
- [4] H. Legoinha. *Measurement of B^\pm meson cross section in pp collisions at the LHC*. LIP-STUDENTS 21-22. LIP, 2021. URL: <https://nc.ncg.ingrid.pt/index.php/s/N68eYHjc5ES6Y8H>.
- [5] J. Ocariz. *Probability and Statistics for Particle Physicists*. URL: <https://cds.cern.ch/record/1701936/files/p253.pdf>.
- [6] S. Costa et al. *Study of B meson production in pp collisions at 5.02 TeV*. Analysis Note. CMS, 2022.
- [7] Maria Faria. *Measurement of B meson production in pp collisions at 5 TeV*. LIP-STUDENTS 20-19. LIP, 2020. URL: <http://cern.ch/lip/pub/docs/LIP-STUDENTS-20-19.pdf>.